J Prosthodont Res. 2023; 67(3): 360–365

OPEN ACCESS

Journal of Prosthodontic Research

Original article

Development of artificial intelligence model for supporting implant drilling protocol decision making

Takahiko Sakai [a,b], Hefei Li [a], Tatsuki Shimada [a], Suzune Kita [a], Maho Iida [a], Chunwoo Lee [a], Tamaki Nakano [b], Satoshi Yamaguchi [a,*], Satoshi Imazato [a]

[a] Department of Biomaterials Science, Osaka University Graduate School of Dentistry, Osaka, Japan, [b] Department of Fixed Prosthodontics, Osaka University Graduate School of Dentistry, Osaka, Japan

Abstract

Purpose: This study aimed to develop an artificial intelligence (AI) model to support the determination of an appropriate implant drilling protocol using cone-beam computed tomography (CBCT) images.

Methods: Anonymized CBCT images were obtained from 60 patients. For each case, after implant placement, images of the bone regions at the implant site were extracted from 20 slices of CBCT images. Based on the actual drilling protocol, the images were classified into three categories: protocols A, B, and C. A total of 1,200 images were divided into training and validation datasets (n = 960, 80%) and a test dataset (n = 240, 20%). Another 240 images (80 images for each type) were extracted from the 60 cases as test data. An AI model based on LeNet-5 was developed using these data sets. The accuracy, sensitivity, precision, F-value, area under the curve (AUC) value, and receiver operating curve were calculated.

Results: The accuracy of the trained model is 93.8%. The sensitivity results for drilling protocols A, B, and C were 97.5%, 95.0%, and 85.0%, respectively, while those for protocols A, B, and C were 86.7%, 92.7%, and 100%, respectively, and the F values for protocols A, B, and C were 91.8%, 93.8%, and 91.9%, respectively. The AUC values for protocols A, B, and C are 98.6%, 98.6%, and 99.4%, respectively.

Conclusions: The AI model established in this study was effective in predicting drilling protocols from CBCT images before surgery, suggesting the possibility of developing a decision-making support system to promote primary stability.

Keywords: Artificial intelligence, Deep learning/machine learning, Computed tomography, Dental implant(s), Prosthodontic dentistry/prosthodontics

Received 20 February 2022, Accepted 12 July 2022, Available online 25 August 2022

1. Introduction

Dental implants have become a significant alternative to reconstruct missing teeth and have revolutionized oral rehabilitation in partially or fully edentulous patients. Implant success depends on biological tissue response and primary stability [1-3]. Primary stability is an important determinant of osseointegration [4,5]. The goal in implant treatment is to obtain the appropriate implant osseointegration to achieve a high rate of long-term success [6-8]. The acquisition of primary stability is important for a better long-term prognosis of implant treatment. Moreover, the volume of bone available for the implant and its quality are highly associated with the type of surgical procedure and the type of implant to be used, and both factors play a vital role in the success of dental implant surgery [9]. The most popular assessment of bone quality was proposed by Zarb [10]; this assessment uses a scale of four classes based on both radiographic assessment and the sensation of resistance experienced by the surgeon. However, this classification has recently been questioned because of its poor objectivity and reproducibility [10,11].

Cone-beam computed tomography (CBCT) has allowed clinicians to view craniofacial structures in three dimensions with high spatial resolution. Computer-assisted surgery (CAS) for implant treatment is a recent advancement that uses CBCT imaging [12]. An assessment of CAS for implant treatment concluded that preoperative assessment improved procedure precision [13]; therefore, the use of CBCT is increasing. In the evaluation of bone quality, Hounsfield units are used for medical computed, and gray values (GVs) are used for CBCT. GVs do not represent actual density values and differ from Hounsfield units [14]. To obtain the appropriate primary stability for an implant, clinicians must decide on the drilling protocols to use and the surgical techniques used for the installation of implants [15,16]. However, it is difficult to determine the best drilling protocol before surgery, especially for young dentists without sufficient surgical experience than senior dentists.

Artificial intelligence (AI) can predict an output from unknown input data by pre-learning the relationship between two known datasets. Deep learning is a type of machine learning approach and is

DOI: https://doi.org/10.2186/jpr.JPR_D_22_00053

***Corresponding author:** Satoshi Yamaguchi, Department of Biomaterials Science, Osaka University Graduate School of Dentistry, 1-8 Yamadaoka, Suita, Osaka 565-0871, Japan.

E-mail address: yamaguchi.satoshi.dent@osaka-u.ac.jp

Table 1. Variations of the patients and their implants

Type	Patient sex	Patient age	Position	Manufacturer	Shape	Diameter (mm)	Length (mm)
A	12 male, 8 female	40-80	12, 15, 26, 35, 36, 37, 46	12 Nobel Biocare, 8 Straumann	9 Straight, 11 Tapered	3.3, 4.1, 4.3, 4.8, 5.0	8.0, 8.5, 10, 11.5, 12
B	6 male, 14 female	32-70	15, 16, 17, 23, 24, 25, 26, 27, 35, 36, 45, 46, 47	13 Nobel Biocare, 7 Straumann	10 Straight, 10 Tapered	3.3, 3.5, 4.1, 4.3, 4.8, 5.0	8.0, 8.5, 10, 11.5, 12
C	4 male, 16 female	19-80	11, 13, 15, 16, 17, 21, 24, 26, 27, 35, 36, 45, 46, 47	17 Nobel Biocare, 3 Straumann	13 Straight, 7 Tapered	3.3, 3.5, 4.3, 4.8, 5.5	7.0, 8.0, 8.5, 10, 11.5

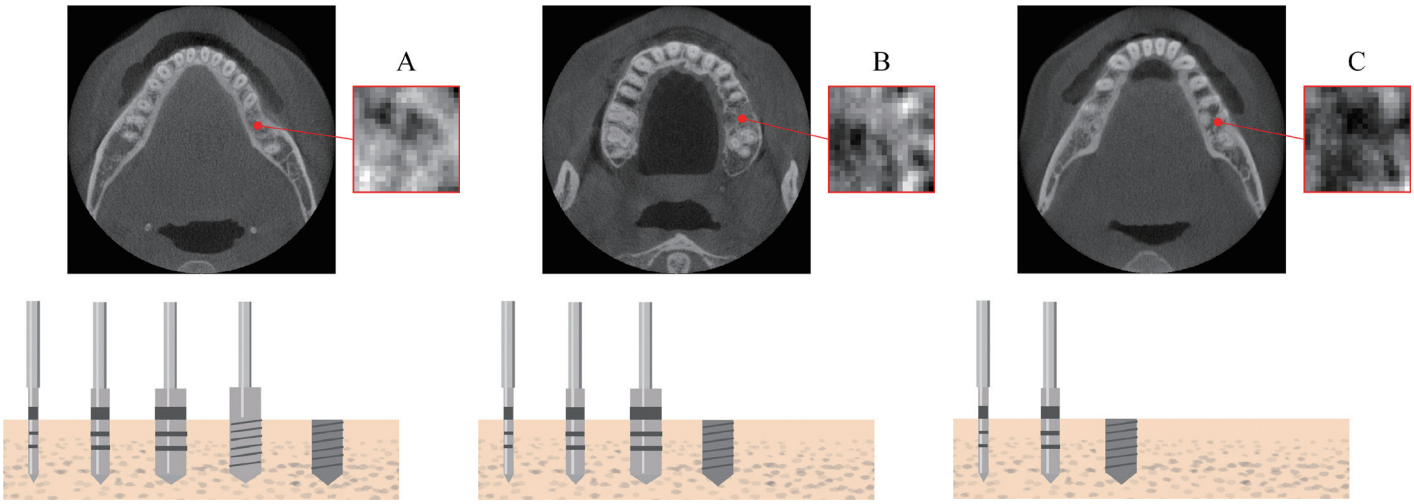

Fig. 1. Examples of cone-beam computed tomography images and the extracted regions of interest for a. patient 7, b. patient 27, and c. patient 59 according to three categories of drilling protocols. A: the conventional drilling protocol with a tapping drill, B: the conventional drilling protocol without a tapping drill, and C: the undersized drilling protocol.

a representation learning method with a complex multilayer architecture. Deep learning derives features from data automatically by transforming the input information into multiple levels of abstraction [17,18]. The success of deep learning in many pattern-recognition applications has led to high expectations that deep learning can bring about revolutionary changes in healthcare. Early studies of deep learning applied to lesion detection and classification have reported superior performance to conventional techniques or even radiologists in computer-aided diagnosis [18]. As the medical field of radiology relies mainly on the extraction of useful information from images, radiology is a natural application area for deep learning, and research in this field has grown rapidly [19,20].

This study aimed to develop an AI model to determine an appropriate implant drilling protocol using CBCT images.

2. Method of research

2.1. Image data sets

This study was conducted in the Department of Fixed Prosthodontics, Osaka University Dental Hospital (approval no. R2-E11). Anonymized CBCT images (512 × 512 pixels in size) were collected from 60 patients who had not received any treatment for bone augmentation or immediate placement of implants (**Table 1**). Patients without sufficient primary stability (30 N/cm), with problems after implant placement within 1 year, and with a risk of osteoporosis were excluded. All CBCT images were taken using AlphardVEGA (ASAHIROENTOGEN, Kyoto, Japan) with a slice thickness of 200 μm and voxel resolution of 200 × 200 × 200.4 μm^3. For each case, bone regions (20 × 20 pixels in size) at the implant site were extracted from 20 slices of the CBCT images after implant placement by a single dentist using ImageJ software (National Institute of Health, Bethesda, MD, USA). The regions of interest (ROIs) of the images were extracted from the bone margin to ensure that an adequate region of cortical bone was included because it has been mentioned in some studies that cortical bone is correlated with primary stability [21]. According to the actual drilling protocol, the images were classified into three categories: A, conventional drilling protocol with a tapping drill; B, conventional drilling protocol without a tapping drill; and C, undersized drilling protocol (**Fig. 1**). Actual drilling protocols were decided by 14 dentists according to the CBCT images before surgery and their hand feeling during surgery. Clinical success was defined as primary stability with a torque exceeding 30 N/cm during surgery and no trouble after implant placement within 1 year. For each protocol, 400 images (20 slices, 20 patients) were prepared.

2.2. Implementation

To implement deep neural networks, the Keras library (version 2.2.4) in Python (version 3.7.2) with a ThinkPad X280 (Core i7-8650 CPU, 16 GB RAM, Lenovo) was used. The software was run on a

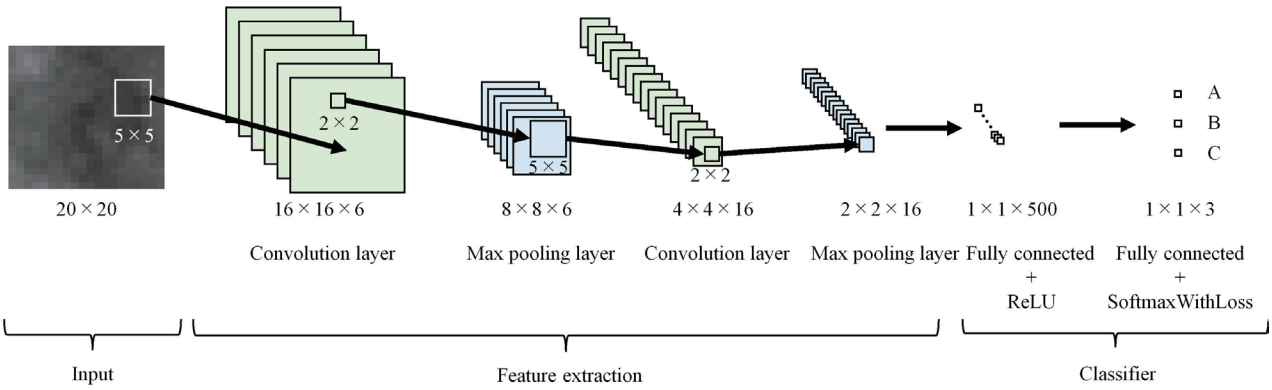

Fig. 2. AI model based on LeNet-5. The feature extraction layer consists of two convolution layers and two max pooling layers. The classifier performs three-class classification according to the predicted drilling protocol A, B, or C.

Windows 11 Pro 64-bit operating system. The training dataset was randomly separated into 64 batches for each epoch, and 50 epochs were run at a learning rate of 0.001. An Adam optimizer was used to train the LeNet-5-based model.

2.3. Structure of the LeNet-5-based model

Figure 2 shows the structure of the LeNet-5-based model used in this study. A total of 1,200 images were divided into training and validation datasets (n = 960 [80%]) and a test dataset (n = 240 [20%]). An equal number of images (16 images for training and validation and four images for testing) were extracted from each case to avoid bias.

2.4. Assessment

The number of true positives (the number of correctly predicted cases of A, B, or C), true negatives (the number of correctly predicted cases of B and C, A and C, or A and B), false positives (the number of incorrectly predicted cases of A, B, or C), and false negatives (the number of incorrectly predicted cases of B and C, A and C, or A and B) was obtained for the 80 test images. Accuracy, sensitivity, precision, and F-value were calculated according to the following equations for each protocol:

$$Accuracy = \frac{True\ positve + True\ negative}{False\ positive + False\ negative + True\ positive + True\ negative}$$

$$Sensitivity = \frac{True\ positive}{True\ positive + False\ negative}$$

$$Precision = \frac{True\ positive}{True\ positive + False\ positive}$$

$$F = \frac{2 \times (Precision \times Sensitivity)}{Precision + Sensitivity}$$

In addition, the area under the curve (AUC) and receiver operating curve (ROC) were obtained for each protocol.

2.5. Visualization

A heat map generated by gradient-weighted class activation mapping (Grad-CAM) [22] was overlaid on a test image to interpret the reason for the predicted protocols.

3. Results

The learning curves are shown in **Figure 3**. After 50 epochs, the accuracy and loss converged. The accuracy of the trained model is 93.7%. Sensitivities for protocols A, B, and C were 97.5%, 95.0%, and 85.0%, respectively. The precision results for protocols A, B, and C were 86.7%, 92.7%, and 100%, respectively, and the F values for protocols A, B, and C were 91.8%, 93.8%, and 91.9%, respectively. The AUC values for protocols A, B, and C were 98.6%, 98.6%, and 99.4%, respectively. The ROCs for protocols A, B, and C are shown in **Figure 4**. Heatmaps generated by Grad-CAM overlaid on the test images are shown in **Figure 5**.

4. Discussion

The AI model based on LeNet-5 developed in this study successfully predicted the drilling protocols of A, B, and C using CBCT images. This is the first step toward predicting the drilling protocol for an implant from CBCT images in prosthodontic dentistry. We believe that the established AI model is useful for decision-making regarding implant drilling protocols, especially for young dentists without sufficient surgical experience.

LeNet-5, developed by LeCun *et al.* [23], is a classic two-dimensional convolutional neural network (CNN) model that has been successfully used in Alzheimer's disease recognition [24] (36,120 images for two classifications, accuracy: 96.85%), traffic sign recognition [25] (51,839 images for six classifications, accuracy: 99.75%), facial expression recognition [26] (981 images for six classifications, accuracy: 97.6%), gas recognition [27] (100 datasets for three classifications, accuracy: 98.76%), pedestrian detection [28] (64,468 images for two classifications, accuracy:75.0%), and other fields [29] (4,056 images for six classifications, accuracy: 86.9%). Compared with these conventional studies, the model established in this study (1,200 images for three classifications, accuracy: 93.7%) achieved high performance even with a smaller dataset. In the case of medical images of 512 × 512 pixels in size, 1,000 test images/classifications are sufficient for prediction with high accuracy [30]. In our study, we extracted images as a region of interest (ROI) of 20 × 20 pixels in size, that is, a 1/655 reduction from the general size of medical images, such as 512 × 512 pixels. The image size used in this study could be one reason for the high performance, even with a small dataset. Because the LeNet-5 network has a relatively simple structure and powerful

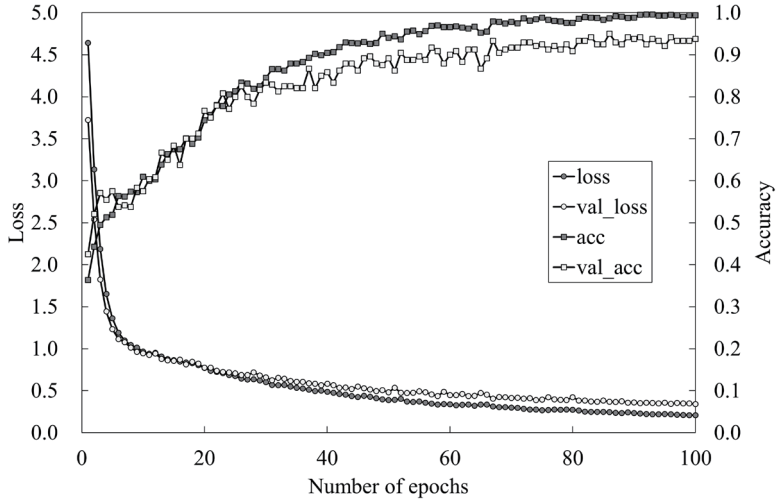

Fig. 3. Learning curves. Rectangular markers indicate accuracy during training. Circular markers indicate the loss of the training data set.

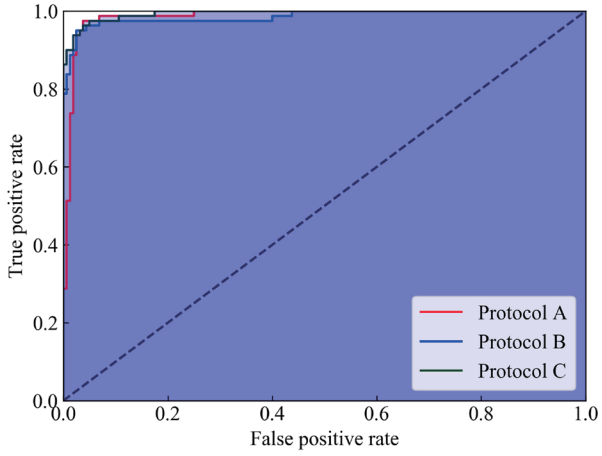

Fig. 4. Recursive operating curves according to three categories of drilling protocols A, B, and C

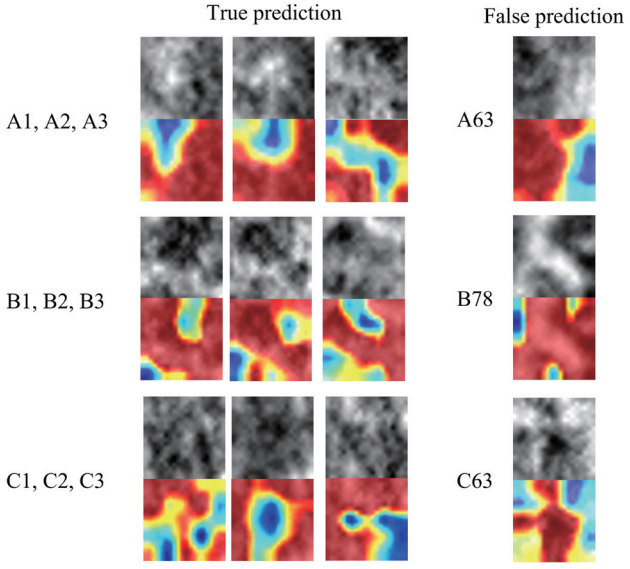

Fig. 5. Test images and heatmap overlaid on these images generated by gradient-weighted class activation mapping (Grad-CAM). Left images of true predictions (drilling protocol A: patient 1, patient 2, and patient 3; drilling protocol B: patient 1, patient 2, and patient 3; and drilling protocol C: patient 1, patient 2, and patient 3) and right images of false predictions (drilling protocol A: patient 63, drilling protocol B: patient 78, and drilling protocol C: patient 63).

classification capability, LeNet-5 was used for CBCT image classification in this study. Recent CNN models, such as GoogleNet [31] and AlexNet [32], have also been considered models for predicting the three drilling protocols. These models have achieved groundbreaking performance in various sophisticated tasks, especially those related to images. Their classification ability often matches or exceeds human performance. The human classification error rate on a large-scale ImageNet dataset was reported to be 5.1% [33], while deep learning achieved an error rate of 3.57% [34]. However, these CNN models were tuned for large color images. Therefore, LeNet-5, which is tuned for monochrome images, such as handwritten characters [23], was employed in this study.

The current prediction accuracy for the 80 test images was 93.7%. Some false predictions occurred because the image features that affect the accuracy of the developed model were limited by the ROI of the implant site, and the ROI could not be expanded further. To increase the number of image features within ROI, super-resolution techniques [35] have been implemented. In addition, the number of cases will gradually increase as data is collected from future patients. Furthermore, a voxel-based 3D-CNN [36] on 3D segmented CBCT images will be useful in increasing the number of image features if more cases can be used as input data.

An image augmentation technique is often used to increase the number of images required to train a CNN model. For the CBCT images, 20 different slices were obtained from each patient, which augmented the total number of samples in the training dataset. For medical images, images of different slices of one patient should generally not be acquired to avoid overfitting because of the similar structural features of adjacent slices. The original CBCT images were 512 × 512 pixels in size; however, the ROIs specified as implant sites were only 20 × 20 pixels in size. The specified ROIs had different structural features, that is, mutual information [37], even in adjacent

Table 2. Confusion matrix with the sensitivity and precision for each drilling protocol. Counts of the estimated/true protocols are colored from 0 (white) to 80 (red).

	Estimated protocols			
True protocols	A	B	C	Sensitivity (%)
A	78	1	1	97.5
B	6	73	1	91.3
C	3	4	73	91.3
Precision (%)	89.7	93.6	97.3	

slices, as shown in the supplemental information (**Figs. S1 and S2**), and hence their use as test images resulted in high accuracy, sensitivity, precision, F-values, and AUC values. The convex shape to the upper left of the ROC curve for each protocol suggests that each drilling protocol correctly predicted a low false prediction.

Within the limitations of this study, the AI model based on LeNet-5 established in this study demonstrated high performance in predicting the three drilling protocols. However, it is still difficult to explain the main factor that induced the misprediction in a few cases (**Table 2 and Fig. 5**). Grad-CAM [22] as an explainable AI method [38] provided us with one of the reasons to visualize the attention regions in the model. The AI model may focus on bone mass in the attention region. The dark region is colored red for protocol A, while the bright region is colored red for protocol C. Interestingly, both visualized patterns were mixed for protocol B. Although it is difficult to clearly distinguish cortical bone from trabecular bone, it is considered that the model focused on trabecular bone in each classification. Due to differences in CBCT equipment, the model in this study was established using only images taken by AlphardVEGA at Osaka University Dental Hospital. Hence, the performance of the model may be uncertain for images captured using other equipment.

5. Conclusions

The AI model established in this study was an effective method of predicting drilling protocols from CBCT images before surgery, suggesting the possibility of developing a decision-making support system to acquire primary stability.

Acknowledgements

We thank Kimberly Moravec, PhD, from Edanz (https://jp.edanz.com/ac), for editing the draft of this manuscript. The authors declare no potential conflicts of interest with respect to the authorship and/or publication of this article.

Conflicts of interest

The authors declare no conflict of interest.

References

[1] Alghamdi H, Anand PS, Anil S. Undersized implant site preparation to enhance primary implant stability in poor bone density: a prospective clinical study. J Oral Maxillofac Surg. 2011;69:e506-12. https://doi.org/10.1016/j.joms.2011.08.007, PMID:22117707

[2] Abrahamsson I, Linder E, Lang NP. Implant stability in relation to osseointegration: an experimental study in the Labrador dog. Clin Oral Implan Res. 2009;20:313-8. https://doi.org/10.1111/j.1600-0501.2008.01646.x, PMID:19405177

[3] Chuang SK, Wei LJ, Douglass CW, Dodson TB. Risk factors for dental implant failure: A strategy for the analysis of clustered failure-time observations. Journal of Dental Research. 2002;81:572-7. https://doi.org/10.1177/154405910208100814, PMID:12147750

[4] Nasatzky E, Gultchin J, Schwartz Z. [The role of surface roughness in promoting osteointegration]. Refuat Hapeh Vehashinayim (1993). 2003;20:8-19, 98. PMID:14515625

[5] Nkenke E, Hahn M, Weinzierl K, Radespiel-Troger M, Neukam FW, Engelke K. Implant stability and histomorphometry: a correlation study in human cadavers using stepped cylinder implants. Clin Oral Implan Res. 2003;14:601-9. https://doi.org/10.1034/j.1600-0501.2003.00937.x, PMID:12969364

[6] Friberg B, Jemt T, Lekholm U. Early failures in 4,641 consecutively placed Branemark dental implants: a study from stage 1 surgery to the connection of completed prostheses. Int J Oral Maxillofac Implants. 1991;6:142-6. PMID:1809668

[7] Lambrecht JT, Filippi A, Kunzel AR, Schiel HJ. Long-term evaluation of submerged and nonsubmerged ITI solid-screw titanium implants: A 10-year life table analysis of 468 implants. Int J Oral Max Impl. 2003;18:826-34. PMID:14696658

[8] Adell R, Eriksson B, Lekholm U, Branemark PI, Jemt T. Long-term follow-up study of osseointegrated implants in the treatment of totally edentulous jaws. Int J Oral Maxillofac Implants. 1990;5:347-59. PMID:2094653

[9] Ekfeldt A, Christiansson U, Eriksson T, Linden U, Lundqvist S, Rundcrantz T, et al. A retrospective analysis of factors associated with multiple implant failures in maxillae. Clin Oral Implants Res. 2001;12:462-7. https://doi.org/10.1034/j.1600-0501.2001.120505.x, PMID:11564105

[10] Zarb GA, Zarb FL. Tissue integrated dental prostheses. Quintessence Int. 1985;16:39-42. PMID:3883391

[11] Shapurian T, Damoulis PD, Reiser GM, Griffin TJ, Rand WM. Quantitative evaluation of bone density using the Hounsfield index. Int J Oral Max Impl. 2006;21:290-7. PMID:16634501

[12] Kernen F, Kramer J, Wanner L, Wismeijer D, Nelson K, Flugge T. A review of virtual planning software for guided implant surgery - data import and visualization, drill guide design and manufacturing. BMC Oral Health. 2020;20:251. https://doi.org/10.1186/s12903-020-01208-1, PMID:32912273

[13] Nickenig HJ, Eitner S. Reliability of implant placement after virtual planning of implant positions using cone beam CT data and surgical (guide) templates. J Cranio Maxill Surg. 2007;35:207-11. https://doi.org/10.1016/j.jcms.2007.02.004, PMID:17576068

[14] Pauwels R, Jacobs R, Singer SR, Mupparapu M. CBCT-based bone quality assessment: are Hounsfield units applicable? Dentomaxillofac Rad. 2015;44. https://doi.org/10.1259/dmfr.20140238, PMID:25315442

[15] Shalabi MM, Wolke JGC, De Ruijter AJE, Jansen JA. Histological evaluation of oral implants inserted with different surgical techniques into the trabecular bone of goats. Clin Oral Implan Res. 2007;18:489-95. https://doi.org/10.1111/j.1600-0501.2007.01362.x, PMID:17517059

[16] Beer A, Gahleitner A, Holm A, Tschabitscher M, Homolka P. Correlation of insertion torques with bone mineral density from dental quantitative CT in the mandible. Clin Oral Implan Res. 2003;14:616-20. https://doi.org/10.1034/j.1600-0501.2003.00932.x, PMID:12969366

[17] LeCun Y, Bengio Y, Hinton G. Deep learning. Nature. 2015;521:436-44. https://doi.org/10.1038/nature14539, PMID:26017442

[18] Chan HP, Samala RK, Hadjiiski LM, Zhou C. Deep Learning in Medical Image Analysis. Adv Exp Med Biol. 2020;1213:3-21. https://doi.org/10.1007/978-3-030-33128-3_1, PMID:32030660

[19] Mazurowski MA, Buda M, Saha A, Bashir MR. Deep learning in radiology: An overview of the concepts and a survey of the state of the art with focus on MRI. Journal of Magnetic Resonance Imaging. 2019;49:939-54. https://doi.org/10.1002/jmri.26534, PMID:30575178

[20] Kurt Bayrakdar S, Orhan K, Bayrakdar IS, Bilgir E, Ezhov M, Gusarev M, et al. A deep learning approach for dental implant planning in cone-beam computed tomography images. BMC Med Imaging. 2021;21:86. https://doi.org/10.1186/s12880-021-00618-z, PMID:34011314

[21] Chavarri-Prado D, Brizuela-Velasco A, Dieguez-Pereira M, Perez-Pevida E, Jimenez-Garrudo A, Viteri-Agustin I, et al. Influence of cortical bone and implant design in the primary stability of dental implants measured by two different devices of resonance frequency analysis: An in vitro study. J Clin Exp Dent. 2020;12:e242-e8. https://doi.org/10.4317/jced.56014, PMID:32190194

[22] Selvaraju RR, Cogswell M, Das A, Vedantam R, Parikh D, Batra D. Grad-CAM: Visual Explanations from Deep Networks via Gradient-Based Localization. Int J Comput Vision. 2020;128:336-59.

[23] Lecun Y, Bottou L, Bengio Y, Haffner P. Gradient-based learning applied to document recognition. P Ieee. 1998;86:2278-324.
[24] Sarraf S, Tofighi G, Neuroimaging AsD. Deep Learning-based Pipeline to Recognize Alzheimer's Disease using fMRI Data. Proceedings of 2016 Future Technologies Conference (Ftc). 2016:816-20.
[25] Cao JW, Song CX, Peng SL, Xiao F, Song SX. Improved Traffic Sign Detection and Recognition Algorithm for Intelligent Vehicles. Sensors-Basel. 2019;19. https://doi.org/10.3390/s19184021, PMID:31540378
[26] Wang G, Gong J. Facial Expression Recognition Based on Improved LeNet-5 CNN. Chin Cont Decis Conf. 2019:5655-60.
[27] Wei GF, Li G, Zhao J, He AX. Development of a LeNet-5 Gas Identification CNN Structure for Electronic Noses. Sensors-Basel. 2019;19. https://doi.org/10.3390/s19010217, PMID:30626158
[28] Zhang CW, Yang MY, Zeng HJ, Wen JP. Pedestrian detection based on improved LeNet-5 convolutional neural network. J Algorithms Comput. 2019;13.
[29] Motta D, Santos AAB, Winkler I, Machado BAS, Pereira D, Cavalcanti AM, et al. Application of convolutional neural networks for classification of adult mosquitoes in the field. PLoS One. 2019;14:e0210829. https://doi.org/10.1371/journal.pone.0210829, PMID:30640961
[30] Cho J, Lee K, Shin E, Choy G, Do S. How much data is needed to train a medical image deep learning system to achieve necessary high accuracy? 2015. p. arXiv:1511.06348.
[31] Szegedy C, Liu W, Jia YQ, Sermanet P, Reed S, Anguelov D, et al. Going Deeper with Convolutions. Proc Cvpr Ieee. 2015:1-9.
[32] Krizhevsky A, Sutskever I, Hinton GE. ImageNet Classification with Deep Convolutional Neural Networks. Commun Acm. 2017;60:84-90.
[33] Russakovsky O, Deng J, Su H, Krause J, Satheesh S, Ma S, et al. ImageNet Large Scale Visual Recognition Challenge. Int J Comput Vision. 2015;115:211-52.
[34] He KM, Zhang XY, Ren SQ, Sun J. Deep Residual Learning for Image Recognition. 2016 Ieee Conference on Computer Vision and Pattern Recognition (Cvpr). 2016:770-8.
[35] Ooi YK, Ibrahim H. Deep Learning Algorithms for Single Image Super-Resolution: A Systematic Review. Electronics-Switz. 2021;10.
[36] Chau RCW, Chong M, Thu KM, Chu NSP, Koohi-Moghadam M, Hsung RT, et al. Artificial intelligence-designed single molar dental prostheses: A protocol of prospective experimental study. PLoS One. 2022;17:e0268535. https://doi.org/10.1371/journal.pone.0268535, PMID:35653388
[37] Seal S, Ghosh D. MIAMI: Mutual Information-based Analysis of Multiplex Imaging data. Bioinformatics. 2022. https://doi.org/10.1093/bioinformatics/btac414, PMID:35748713
[38] Gunning D, Stefik M, Choi J, Miller T, Stumpf S, Yang GZ. XAI-Explainable artificial intelligence. Sci Robot. 2019;4. https://doi.org/10.1126/scirobotics.aay7120, PMID:33137719